TOXICOLOGICAL SCIENCES **114(2)**, 310–322 (2010)
doi:10.1093/toxsci/kfq002
Advance Access publication January 8, 2010

Chronic Exposure to Manganese Alters Brain Responses to Amphetamine: A Pharmacological Magnetic Resonance Imaging Study

Jason M. Williams,*,† Dejan Milatovic,‡ John C. Gore,*,†,§ Michael Aschner,‡,§,¶,||,||| and Malcolm J. Avison*,†,§,¶,[1]

*Department of Radiology and Radiological Sciences; †Vanderbilt University Institute of Imaging Science; ‡Department of Pediatrics; §Kennedy Center for Research on Human Development; ¶Department of Pharmacology; ||Center for Molecular Neuroscience; and |||Center in Molecular Toxicology, Vanderbilt University Medical Center, Nashville, Tennessee 37232

[1] To whom correspondence should be addressed at Vanderbilt University Institute of Imaging Science, Vanderbilt University Medical Center, 1161 21st Avenue South, AA-3101 Medical Center North, Nashville, TN 37232. Fax: (615) 322-0734. E-mail: calum.avison@vanderbilt.edu.

Received October 6, 2009; accepted December 19, 2009

The parkinsonian symptoms and increased Mn accumulation in dopaminergic (DAergic) neurons of the basal ganglia implicate impaired dopamine signaling in the neurotoxic effects of chronic manganese overexposure. Using blood oxygenation level–dependent (BOLD) pharmacological magnetic resonance imaging (phMRI), we mapped brain responses to acute amphetamine (AMPH; 3 mg/kg, ip), which stimulates midbrain DAergic systems, in male Sprague-Dawley rats following 6 weeks of chronic $MnCl_2$ (5 mg Mn/kg, one per week, iv) or saline treatment. Plasma Mn content, measured immediately following phMRI, was elevated twofold in Mn-treated animals ($p < 0.05$), but the twofold increase in mean striatal Mn content did not reach significance. In saline-treated animals, AMPH stimulated robust positive BOLD responses throughout the basal ganglia and their reciprocally innervated connections. In contrast, acute AMPH stimulated a negative BOLD response in many of these structures in the Mn-treated group, resulting in significant differences between saline- and Mn-treated AMPH-evoked BOLD responses within caudate putamen, globus pallidus, substantia nigra, mediodorsal thalamic nucleus, and somatosensory cortex. These results demonstrate the utility of AMPH-evoked phMRI as readout of the DAergic signaling *in vivo* and confirm the vulnerability of DAergic systems to Mn.

Key Words: **manganese; Parkinson's disease; dopamine; basal ganglia; neurodegeneration; magnetic resonance imaging.**

Manganese (Mn) is a naturally occurring element and essential dietary nutrient that is involved in numerous physiological processes, including lipid, carbohydrate and protein metabolism, immune system function, blood clotting, and osteogenesis (Aschner *et al*., 2007). Mn serves as a cofactor for a variety of antioxidant and metabolic enzymes, such as Mn superoxide dismutase (Mn-SOD), pyruvate carboxylase, arginase, and glutamine synthetase (Aschner *et al*., 2007; Takeda, 2003). At physiological concentrations, Mn plays a critical role in neuronal homeostasis and synaptic transmission (Aschner and Aschner, 1991; Narita *et al*., 1990; Takeda *et al*., 2002).

Mn is abundant in the environment and is one of the most common metals found in commercial products and industrial settings. It is consumed in the production of steel and in various welding applications, while lesser amounts are typically used in the manufacture of various batteries and antimicrobial compounds as well as in water purification (Perl and Olanow, 2007). The widespread environmental availability and commercial access to Mn have led to concerns related to excessive exposure and potential toxicity. Increased Mn body burden has been documented upon exposure to maneb-adulterated food (Ferraz *et al*., 1988), administration of Mn-SOD mimetics (EUK-8) (McDonald *et al*., 2003), iv use of the euphoric stimulant, methcathinone (Stepens *et al*., 2008), as well as potassium permanganate (Xu *et al*., 2005). Occupational exposures occur in mining, steel manufacturing, and welding (Pal *et al*., 1999; Racette *et al*., 2001, 2005).

The clinical manifestations of Mn intoxication are similar to those observed in patients with idiopathic Parkinson's disease (PD). Exposure to high levels of Mn, which are common in industrial and/or occupational settings, can produce considerable neurobehavioral toxicity with symptoms ranging from psychiatric disturbances (depression, hallucinations, and agitation) to locomotor deficits akin to symptoms found in PD (Aschner *et al*., 2007; Perl and Olanow, 2007). In addition, Mn has been shown to exacerbate the susceptibility and expression of existing PD motor and behavioral symptoms, including rigidity, bradykinesia, abnormal gait, and dystonia (Perl and Olanow, 2007). Exposure to high levels of Mn is also known to cause decrements in cognitive abilities, including impaired learning, memory, and sensorimotor information processing (Aschner *et al*., 2007). Depending on the level of Mn exposure, these symptoms often coalesce to form a syndrome called "manganism" that has a clinical expression nearly indistinguishable from idiopathic PD.

Biomedical imaging *in vivo* provides new insights into the neuropathology associated with manganism (Kim, 2006).

Positron emission tomography (PET) studies in nonhuman primates have made use of an 18F-labeled form of the tyrosine hydroxylase substrate levodopa ([^{18}F]DOPA) as an index of dopamine (DA) synthesis and thus an indirect readout for the functional integrity of the nigrostriatal pathway (Brooks *et al*., 1990; Leenders *et al*., 1990). Using [^{18}F]DOPA PET, a significant (40–60%) reduction in nigrostriatal dopaminergic (DAergic) neuronal function was observed in PD patients (Brooks *et al*., 1990; Leenders *et al*., 1990). In contrast, in nonhuman primates and humans chronically exposed to Mn, there is little evidence of significant neurodegeneration of nigral DA neurons (Perl and Olanow, 2007), and the integrity of the nigrostriatal system remains relatively intact (Eriksson *et al*., 1992b; Shinotoh *et al*., 1995, 1997; Wolters *et al*., 1989). Although there is little evidence of loss of DAergic neurons, recent studies in nonhuman primates do suggest that both presynaptic and postsynaptic elements of DA neurotransmission may be affected by Mn. Thus, acute Mn increases striatal dopamine transporter (DAT) levels, while chronic Mn exposure is associated with impaired amphetamine-stimulated (AMPH) DA release despite a normalization of DAT levels (Burton and Guilarte, 2009; Guilarte *et al*., 2006, 2008) and reduced postsynaptic DA D1 receptor levels. These and other findings suggest that while both idiopathic PD and manganism target midbrain nigrostriatal DA systems, the Parkinsonian features of Mn-induced central nervous system (CNS) dysfunction may arise, at least in part, from the impact of disrupted DA neurotransmission on downstream neural pathways rather than neurodegeneration *per se* (Calne *et al*., 1994; Huang *et al*., 1998; Olanow, 2004).

Molecular/nuclear imaging studies in humans and nonhuman primates, particularly PET, have provided important information on the effects of chronic Mn exposure on different elements of DA neurotransmission, including rates of DA synthesis, release and the levels of the DAT, and presynaptic and postsynaptic receptors. They are, however, limited in their ability to probe the downstream functional consequences of any disruption in DA signaling and generally have rather low temporal and spatial resolution. In contrast, functional magnetic resonance imaging (fMRI), which maps changes in local blood oxygenation (so-called blood oxygenation level–dependent [BOLD] contrast; Ogawa *et al*., 1990) or blood volume, associated with changes in local neural activity, lacks molecular specificity but has high spatial and temporal resolution, and in the case of BOLD fMRI requires no exogenous tracer or contrast agent to perform functional brain mapping (Muller-Gartner, 1998; Steward *et al*., 2005).

fMRI is now routinely exploited for functional brain mapping in humans (Arthurs and Boniface, 2002; Buxton *et al*., 2004; Gore, 2003; Logothetis, 2003; Logothetis and Pfeuffer, 2004) and is increasingly used in animals and humans to map the patterns of altered CNS activity associated with a direct pharmacological challenge and variant sometimes referred to as "pharmacological magnetic resonance imaging" or "phMRI" (Wise and Tracey, 2006). This technique has been used to examine the central effects of psychostimulant compounds such as cocaine and AMPH that target DAergic systems of the brain (Chen *et al*., 1997, 1999; Dixon *et al*., 2005; Easton *et al*., 2007). Notably, comparing *in vivo* microdialysis, PET and phMRI data from recent studies have demonstrated that the AMPH-induced BOLD response is correlated with AMPH-evoked increases in DA transmission within the caudate putamen (CPu) (Chen *et al*., 1997, 1999), an area that together with other basal ganglia (globus pallidus [GP], subthalamic nucleus [STh], and substantia nigra [SN]) are sensitive to Mn-induced neurotoxicity (Aschner *et al*., 2007). The purpose of the current study was to demonstrate that whole-brain measurement of the AMPH-induced BOLD signal change—detected with fMRI—could provide readout for the relative functional responsiveness of neural pathways and transmitters dysregulated as a consequence of repeated exposure to Mn as well as advance the mechanistic understanding on the role of DA in Mn-induced neurodegeneration.

MATERIALS AND METHODS

Animals. All methods were approved by the Vanderbilt University Medical Center's Institutional Animal Care and Use Committees and were conducted in accordance with the National Institutes of Health *Guide for the Care and Use of Laboratory Animals*. Male Sprague-Dawley rats (~300 g; Harlan, Indianapolis, IN) were given free access to food and water throughout the duration of the study. After habituation to the vivarium (4–6 days), animals were divided into chronic saline and Mn pretreatment groups ($n = 7$). Animals received weekly iv tail vein injections of $MnCl_2$ (5 mg Mn/kg) or isotonic saline vehicle (1 ml/kg) for a total of 6 weeks. This dosing regimen produces elevations in blood Mn known to underlie neurobehavioral deficits in humans exposed environmentally to Mn (Mergler, 1999; Park *et al*., 2003). Rat body weights were recorded weekly. Animals underwent functional imaging 1 week after the last weekly Mn/saline injection. Blood and brain samples were collected for further analysis of Mn content (see below) at the conclusion of the magnetic resonance imaging (MRI) scans to assess Mn accumulation in plasma and striatum.

Physiology. All procedures related to magnetic resonance (MR) scans were adapted from those used in a previous study (Williams *et al*., 2007). After 6 weeks of repeated systemic Mn injections, animals were surgically prepared to undergo fMRI. On the day of the MR scan, animals were implanted with a femoral artery catheter (PE50 tubing, 15 cm) for measurement of blood pressure, an ip catheter (PE50 tubing, 15 cm) for administration of drug solutions, and an endotracheal tube (14 gauge, 2 cm) to accommodate artificial respiration under continuous isoflurane (2%) anesthesia. After surgeries, animals were transferred to a customized stereotaxic frame with adjustable Teflon ear and incisor bars to support the skull and minimize motion during scanning. A 20-mm transmit/receive radio frequency (RF) surface coil (Varian Instruments, Palo Alta, CA) was positioned < 1 mm above the scalp. Animals were ventilated by connecting the endotracheal tube to a 2-cm Y-shaped adapter joined to two flexible silicone inhalation/exhalation line, each 4 m in length and connected to a mechanical pressure–controlled ventilator (Kent Scientific, Litchfield, CT) attached to a two-gas mixer; both the all ventilation equipment were housed in a anteroom adjacent to the magnet room, ~3 to 4 m from isocenter. During the prescan preparations, ventilation settings were adjusted (respiratory rate = 51–55 breaths/min; peak inspiration volume 18–20 cm H_2O) to maintain stable physiologic conditions. All animals were subject to real-time monitoring of end-tidal carbon dioxide ($EtCO_2$)—an indirect measure

of arterial pCO_2—via a SurgiVet V9004 capnograph (Waukesha, WI) connected to the endotracheal tube/Y-tube coupling. Under these conditions, there were no significant differences in $EtCO_2$ (average of last 60 s prior to AMPH injection, expressed as millimeter of mercury) between saline- versus Mn-pretreated animals: 25.8 ± 1.93 (saline, $n = 5$) versus 22.5 ± 1.73 (Mn, $n = 6$), $p = 0.234$, $t = 1.28$ ($df = 9$), respectively, unpaired two-tailed Student's t-test.

The carrier gas mixture was changed from 2% isoflurane in 100% oxygen during surgical preparation to 0.8% isoflurane in 30% oxygen: 70% nitrous oxide mixture after transferring the animal to the stereotaxic frame. Once stabilized in the holder, rats received a bolus injection of pancuronium bromide (2 mg/kg, ip; Sigma, St Louis, MO) to induce musculoskeletal paralysis necessary to suppress resistance to stable mechanical ventilation. A pneumatic pillow (SA Instruments, Stony Brook, NY) was positioned underneath the animal's abdomen to monitor respiration, which was maintained at ~50 breaths/min. Rectal body temperature, heart rate (electrocardiogram), and respiration rate were continuously recorded using an MRI-compatible monitoring and gating system (SAM-PC; SA Instruments) that controlled a thermocoupled heating unit for maintenance of body temperature at 37–38°C. In a subset of animals from both treatment groups, mean arterial blood pressure (MAP) was monitored with a blood pressure transducer (Hospira Transpac IV, Lake Forest, IL) attached to the femoral arterial catheter. In these animals, there appeared to be no significant differences in MAP as a function of pretreatment (average of last 60 s prior to AMPH injection, expressed as millimeter of mercury): 99.0 ± 10.3 (saline, $n = 3$) versus 113 ± 7.51 (Mn, $n = 3$), $p = 0.333$, $t = 1.10$ ($df = 4$), unpaired two-tailed Student's t-test. A microbore extension set (0.2 ml residual volume) was attached to the ip catheter to allow injection of drugs from outside the MR scanner room.

Functional MR image acquisition. All MRI studies were performed using a 7.0 Tesla Varian Inova small animal scanner equipped with actively shielded gradients (27 G/cm; 100-μs rise time) running VnmrJ v6.1D software and a 20-mm surface transceiver coil positioned 1 mm above the scalp. Prior to acquisition of the functional image series, a set of higher resolution anatomic images were acquired using a gradient echo multislice (GEMS) pulse sequence having the following parameters: repetition time (TR) = 200 ms, echo time (TE) = 8 ms, flip angle = 27°, number of excitations (NEX) = 4, slice thickness = 1.5 mm (nine slices, no gap), in-plane resolution = 0.12 × 0.12 mm, matrix = 256 × 256, field of view (FOV) = 30 × 30 mm, and acquisition time = 38 s. Next, a series of 90 consecutive BOLD-sensitized functional image volumes, spatially aligned with the anatomic images, was acquired, using the same GEMS sequence with acquisition parameters modified to provide transverse relaxation time ($T2^*$) weighted (BOLD) contrast: TR = 300 ms, TE = 18 ms, flip angle = 33°, NEX = 2, slice thickness = 1.5 mm (nine slices, no gap), in-plane voxel resolution = 0.47 × 0.47 mm, matrix = 64 × 64, FOV = 30 × 30 mm, and acquisition time = 38.4 s. After collection of 30 predrug baseline images, a bolus infusion of AMPH (3 mg/kg, ip; delivered in isotonic saline vehicle, 1 ml/kg) was given via the microbore extension set over an infusion time of ~30 s. An additional 60 post-AMPH functional images were acquired without interruption for a total functional imaging run duration of ~1 h.

Blood collection and brain tissue dissection. Immediately following the MR scans, rats were given an injection of ketamine (80 mg/kg, ip) with xylazine (12 mg/kg, ip) to induce deep anesthesia and subsequently decapitated. Trunk blood was collected in heparinized tubes and placed on ice. Trunk blood was subsequently centrifuged (1000 × g) at 4°C for 30 min to separate red blood cells from plasma and stored at −80°C. The brains were excised, and the striatum was blunt dissected, rapidly frozen on dry ice, and stored at −80°C.

Atomic absorption spectroscopy. Quantification of Mn in plasma and the dissected brain tissue specimen was conducted with a graphite furnace atomic absorption spectrometer (GFAAS; model AA240; Varian, Inc.) according to previously described methods (Fitsanakis *et al*., 2008). Briefly, brain tissues were first digested by dilution in nitric acid (1:10 wt/vol) for ~48 h in a sand bath at 60°C. Digested tissue (100 μl) was diluted to 1 ml with 2% nitric acid and analyzed for Mn. Plasma (400 μl) aliquots were vigorously mixed with 0.5% Triton-X (100 μl) for 30 s and brought to a final volume of 1 ml with 2% nitric acid. This mixture was then centrifuged, and a portion of the resulting supernatant (100 μl) was further diluted to a 1 ml volume with 2% nitric acid and analyzed for Mn. For GFAAS determinations of Mn concentration, bovine liver (10 μg Mn/l) was digested in ultrapure nitric acid and included as an internal standard.

MRI data analysis. MR data were analyzed using AFNI (Cox, 1996) (http://afni.nimh.nih.gov/afni). Functional data from each subject were coregistered using rigid body alignment to a template multislice image set that was selected from one of the saline-pretreated control subjects. Registered image intensities were converted to a percentage BOLD signal change relative to a pre-AMPH baseline period ($\%\Delta S/S_0$) on a per-voxel basis. Data were further processed by linear detrending over the baseline period to correct for nondrug-related signal drifts. Processed images from each pretreatment condition were group averaged and aligned with a high-resolution anatomic underlay acquired from the same subject as the functional template overlay described above. To create group activation maps, individual post-AMPH time series data were integrated and the resulting area under curve (AUC) was calculated for each voxel. Saline- versus Mn-treated group AUCs were compared on a voxel-wise basis using the Student's t-test. The statistical threshold for significance was set to a value of t corresponding to $p < 0.05$ in AFNI using the *3dttest* batch program. Additional group activation maps were created by computing the mean $\%\Delta S/S_0$ for the last 24 images (15 min) in the post-AMPH interval. This period encapsulated the peak AMPH-induced signal change for the saline-pretreated control group and encompasses the time course of action for neuropharmacologic and motor stimulant effects of AMPH (Dixon *et al*., 2005; Sulzer *et al*., 2005). To examine the temporal structure of the AMPH-induced BOLD response, region of interest (ROI) analysis was conducted across a number of different brain areas thought to be involved in the neuropathology of manganism and PD and which are also known substrates for AMPH in the CNS. Using a standard stereotaxic rat brain atlas as a guide (Paxinos and Watson, 1998), ROIs were drawn with the "draw data set" plug-in within AFNI over several structures throughout the basal ganglia, limbic system, and neocortex (see below). Time series data from each ROI were averaged across left and right hemispheres. Post-AMPH BOLD responses in saline- and Mn-treated subjects were integrated, averaged across treatment groups, and analyzed by a Student's t-test. Group differences in the post-AMPH AUC for each ROI were considered significant at $p < 0.05$.

GFAAS and physiologic data analyses. Plasma and brain tissue concentrations of Mn in saline- versus Mn-treated subjects were compared using the Student's t-test with a significance level of $p < 0.05$. Body mass data collected over the duration of the 6-week Mn treatment period were analyzed by linear regression analysis, followed by t-test comparison of the regression lines (GraphPad Prism v4.03, San Diego, CA).

RESULTS

Body Mass

Throughout the duration of the 6-week Mn treatment regimen, animals were weighed weekly to assess general health. Animals were also routinely observed (three times per week) for the expression of any obvious behavioral manifestations. Similar to previous findings (Fitsanakis *et al*., 2008), the 6-week low-dose Mn regimen used in the current study (5 mg Mn/kg/week) did not result in the expression of any overt behavioral abnormalities. Furthermore, as shown in Figure 1, there were no significant differences in body mass between Mn- and saline-treated control subjects in any particular time point nor were there significant differences in the growth rates between the two groups. The study by Fitsanakis *et al*. (2008)

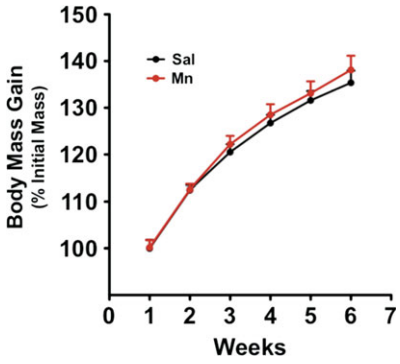

FIG. 1. Weekly body mass gain. Rats were weighed weekly as a general assessment of overall health. No significant difference ($p > 0.05$) in weight between saline-exposed (control) and manganese-exposed (Mn) animals were seen during the treatment period (6 weeks).

utilized a 14-week Mn regimen (5 mg/kg, ip) and found that Mn-treated subjects displayed a significant decrease in body mass after the regimen. However, in that report, as with the present study, there were no significant Mn-induced changes in body mass within the first 6 weeks of treatment.

Mn Levels in Plasma

Previous studies have shown that Mn readily binds to and is transported throughout the body by a number of plasma proteins (Mahoney and Small, 1968). Thus, using GFAAS, we evaluated Mn content within Mn- versus saline-treated animals in plasma samples obtained from trunk blood collected immediately after the completion of MR scans, i.e., 1 week following the last of the six weekly $MnCl_2$ injections. As shown in Figure 2A, compared to saline-treated control animals, the 6-week Mn treatment regimen resulted in an approximate twofold increase in plasma Mn: saline-treated animals 7.10 ± 1.15 μg Mn/l plasma ($n = 5$) and Mn-treated animals 14.16 ± 1.76 μg Mn/l plasma ($n = 7$), $p = 0.0122$, $t = 3.054$, $df = 10$. These results are consistent with other reports, e.g., Al-Bader *et al.* (1997) reported similar levels of plasma Mn in control animals.

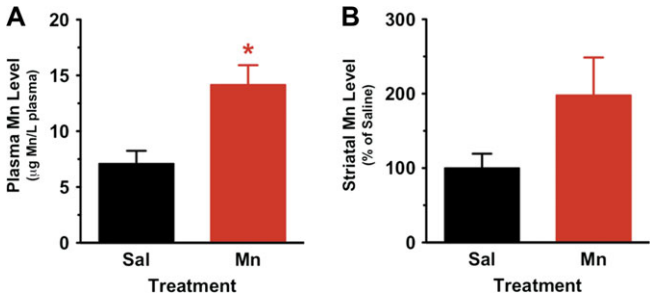

FIG. 2. Mn levels in plasma and striatum of saline-exposed (control) and manganese-exposed (Mn) animals. (A) GFAAS was used to determine the amount of Mn in plasma from rats at the last week of study (6 weeks). Mn content was statistically significantly increased ($p < 0.05$) in plasma of rats exposed to Mn compared to saline-injected animals. (B) GFAAS was used to determine the amount of Mn in striatal brain tissue samples obtained from rats at the last week of study (6 weeks). Values are expressed as percent change from control (mean ± SEM for Mn levels in striatum of saline-exposed rats is 350.30 ± 139.10 nmol/g tissue). Twofold increases in Mn content was seen in striatum of rats exposed to Mn compared to saline-injected animals, but the difference was not statistically different.

Mn Levels in Striatal Tissue

Previous data suggest that Mn preferentially accumulates in the basal ganglia and, in particular, the CPu (Newland *et al.*, 1989; Perl and Olanow, 2007). Moreover, this region is enriched with nerve terminals from the nigrostriatal pathway and contains a dense distribution of the DAT (Nirenberg *et al.*, 1996), which is the primary target of AMPH-like psychomotor stimulants (Sulzer *et al.*, 2005). While the chronic Mn regimen did result in an approximate twofold increase in striatal Mn content (Fig. 2B), the difference did not reach statistical significance: saline-treated animals 350.3 ± 139.1 nmol/g tissue ($n = 5$) and Mn-treated animals 693.3 ± 366.5 nmol/g tissue ($n = 6$), $p = 0.1298$, $t = 1.667$, $df = 9$.

Group Map of AMPH-Induced BOLD Response in Mn- and Saline-Treated Subjects

Figure 3 shows group maps that depict how the two pretreatment conditions (Mn vs. saline) differed. Maps were overlaid on high-resolution multislice images (Fig. 3A) obtained in the same animal used for the lower-resolution functional template. Group statistical maps—showing the average AUC for each group—reveal several clusters of voxels (red) that represent significant (uncorrected Student's t-test = 2.201; per-voxel $p < 0.05$) differences in the AMPH-induced BOLD response between Mn- and saline-treated control subjects (Fig. 3B). No significant group difference in baseline temporal signal-to-noise ratio (SNR), computed as mean/SD of the pre-AMPH baseline period for every image voxel, was found between Mn- and saline-treated rats (Fig. 3C). Figures 3D and 3E show maps of the group mean BOLD signal changes in response to AMPH injection for saline-treated (Fig. 3D) and Mn-treated (Fig. 3E) rats. The average $\%\Delta S/S_0$ spanning the last 15 min (24 images) of the post-AMPH period was calculated on a per-voxel basis for each subject. In controls that received repeated weekly injection of saline, the AMPH challenge elicited a widespread BOLD signal increase throughout cortex, basal ganglia, thalamus, and the limbic system (Fig. 3D). Surprisingly, a slight reduction below baseline in the AMPH-induced BOLD signal change was observed in the anterior medial prefrontal cortex (mPFC-A) and surrounding areas within saline-treated control subjects (Fig. 3D). In marked contrast to these effects, Mn-treated rats exhibited widespread reductions in BOLD signals after AMPH challenge in many of these same areas (Fig. 3E). In addition, the mean AMPH-induced BOLD response in the mPFC-A and adjacent areas appeared to be decreased by a greater degree within Mn-treated compared to saline-treated animals (Fig. 3E).

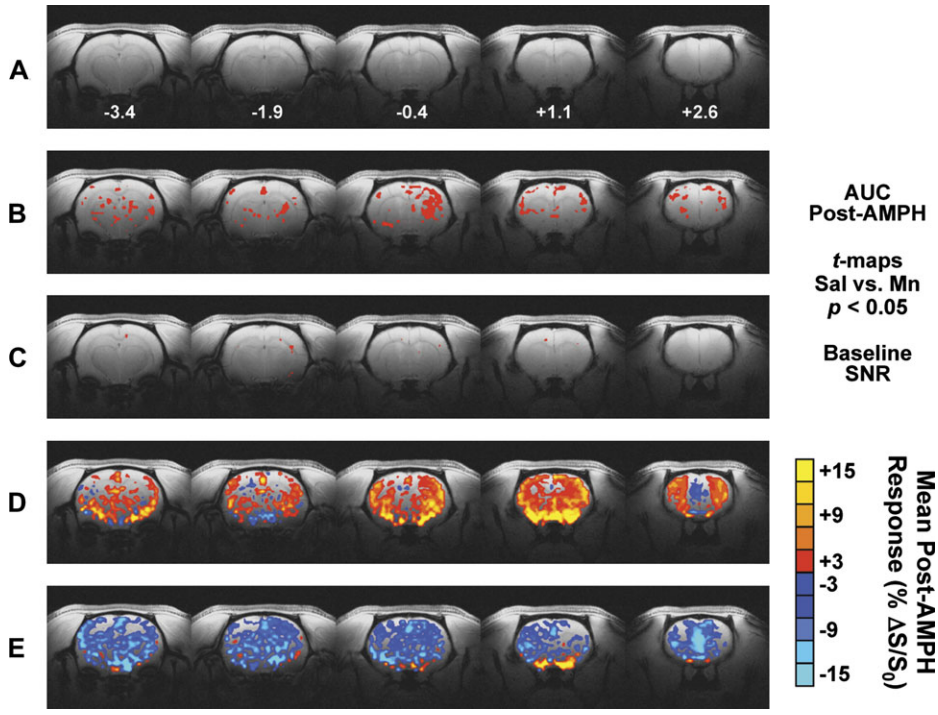

FIG. 3. Group-averaged map of the BOLD response to AMPH within saline- and Mn-treated subjects within five contiguous coronal slices imaged with phMRI. (A) Anatomic template used as underlay for creation of activation maps. Below each image slice is the approximate rostrocaudal stereotaxic distance from bregma (in millimeters) (Paxinos and Watson, 1998). (B) The entire 60-image post-AMPH percent change in BOLD signal relative to baseline ($\%\Delta S/S_0$) was integrated for each subject, and the resulting AUC from all subjects in each treatment group (sal vs. Mn) were compared on a per-voxel basis using the Student's *t*-test. Red voxels represent significant differences between sal versus Mn groups (t threshold = 2.201, $p < 0.05$). (C) SNR comparisons for sal- versus Mn-treated groups. (D and E) Colorized BOLD activation maps show the mean per-voxel $\%\Delta S/S_0$ for the last 15 min of the post-AMPH period (images 76–90) for sal-treated (D) and Mn-treated (E) subjects. The minimum level of activation for the maps in panels D and E is 3%.

The original size of the Mn pretreatment group in the current imaging studies was $n = 8$. Within-subjects inspection of individual raw and postprocessed time series data revealed one Mn-treated subject that exhibited an AMPH-induced BOLD signal change (AUC) exceeding 2 SDs of the mean response for the seven remaining Mn-treated animals. This animal was subsequently removed from the final Mn treatment group. The group mapping in Figure 3 above and ROI analyses below were conducted using final group sizes of $n = 7$ (Mn treated) and $n = 6$ (saline treated).

ROI Analysis of BOLD phMRI Data in Mn- and Saline-Treated Subjects

Placement of ROIs. The maps in Figure 3 represent qualitative comparisons of the responses to AMPH challenge within Mn- versus saline-treated animals and as such provide limited information about the effects of Mn treatment on hemodynamic end points. A complementary analysis that provides more quantitative assessment in a particular brain area compares drug-induced BOLD responses within predefined ROIs. We were interested in examining more closely those structures that are targets of Mn deposition/accumulation, those that play important roles in PD and manganism, and/or those that are known monoaminergic (DA and norepinephrine) substrates for psychostimulants, such as AMPH. Thus, ROIs were selected from the nigrostriatal and mesocorticolimbic DA systems as well as other cortical and subcortical structures that are interconnected with these systems. Figure 4 shows the position of the ROIs, colorized and overlaid onto a high-resolution anatomic background template, that were analyzed in the current study. ROIs were drawn within AFNI using the Paxinos and Watson (1998) rat brain stereotaxic atlas as an anatomical guide.

Basal ganglia. The basal ganglia are critically involved in a variety of functions, such as motor control, cognition and learning, attention, and emotion (Cotterill, 2001; Wichmann and DeLong, 2003). Some of these functions are, to varying degrees, disrupted as a result of Mn exposure, and these structures appear to be primary Mn deposition sites that undergo progressive neurodegeneration with PD and manganism (Aschner *et al.*, 2007; Takeda, 2003). Figure 5 compares the time course of the BOLD response to AMPH in ROIs delineating the four nuclei that comprise the basal ganglia: the CPu (Fig. 5A), GP (Fig. 5B), STh (Fig. 5C), and substantia nigra compacta (SNc; Fig. 5D). Inspection of time series data from all four structures showed that Mn-treated animals exhibited a negative BOLD response to systemic AMPH challenge that was maintained for the duration of the scan (> 30 min). When time series data from these ROIs were integrated,

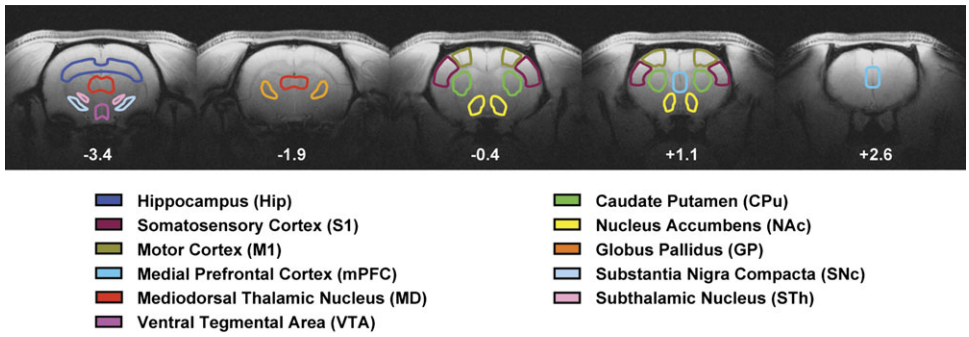

FIG. 4. Placement of ROIs for quantitative assessment of the effects of chronic manganese on the AMPH-induced BOLD signal change. These structures represent the key basal ganglia, mesocorticolimbic, cortical, and subcortical sites that either are targets of Mn accumulation and PD pathophysiology or are key monoaminergic nuclei involved in the neural actions of AMPH. Below each image slice is the approximate rostrocaudal stereotaxic distance from bregma (in millimeters) (Paxinos and Watson, 1998).

CPU, GP, and SNc exhibited a significant ($p < 0.05$ vs. saline pretreatment) negative AUC post-AMPH (Figs. 5A, 5B, and 5D, insets). While the STh exhibited a similar trend in Mn-treated animals, the AUC comparison to saline did not reach statistical significance.

Cortex and thalamus. The cerebral cortex and thalamus have significant reciprocal connections with the basal ganglia, and the integrity of motor cortex (M1) motor and somatosensory cortex (S1) somatosensory cortical signals to and from the basal ganglia play a key role in production of coordinated motor output. AMPH induced a clear increase in the BOLD signal in both M1 and S1 of the saline-pretreated control group, an effect that was absent in the chronic Mn-treated group (Figs. 6A and 6B), which again showed a trend toward a negative BOLD response. Analysis of the post-AMPH AUC showed that the differential effect of pretreatment (Mn vs. saline) reached statistical significance ($p < 0.05$) in S1 but not in M1. The thalamus, including the mediodorsal thalamic nucleus (MD), receives input from the basal ganglia as well as providing excitatory output to prefrontal cortical areas involved in movement, reward, and cognition. The hippocampus also exerts a major influence on prefrontal cortex and plays a key role in the memory-impairing effects of Mn exposure. In spite

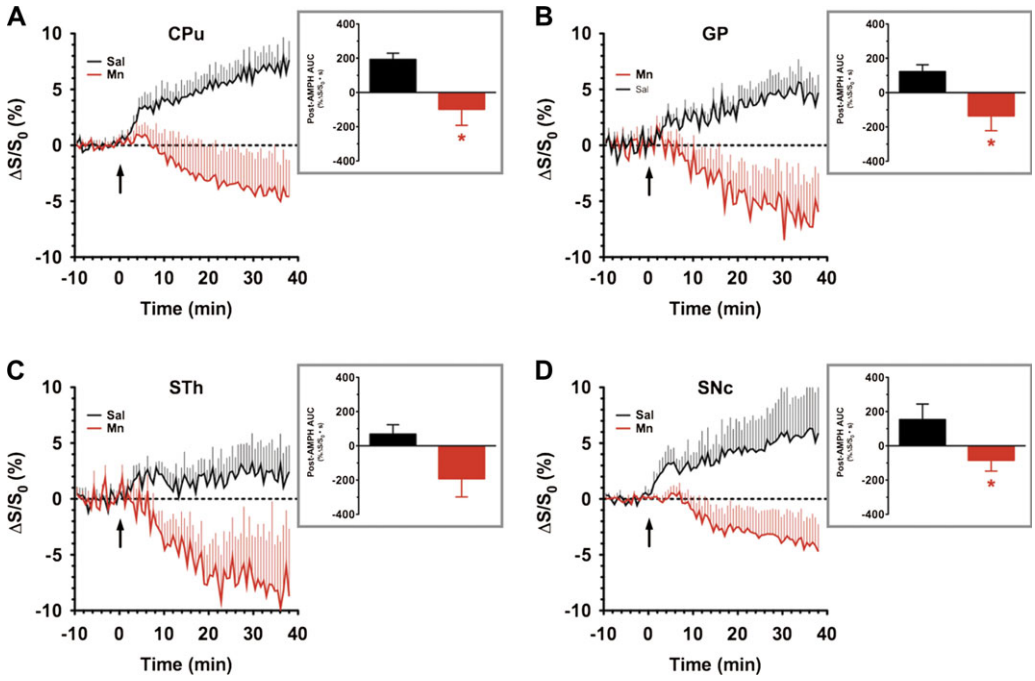

FIG. 5. ROI analyses of BOLD phMRI data obtained within the basal ganglia of saline- versus chronic Mn-treated subjects. Time series data represent mean $\%\Delta S/S_0$ in the ROI in response to AMPH injection (3 mg/kg, iv, arrow): (A) CPu, (B) GP, (C) STh, and (D) SNc. Insets: Integration of post-AMPH time series data reveals a statistically significant decrease in the AMPH-induced BOLD response within the CPu, GP, and SNc (AUC, $\%\Delta S/S_0 \bullet s$). Saline versus Mn: $^*p < 0.05$, Student's *t*-test.

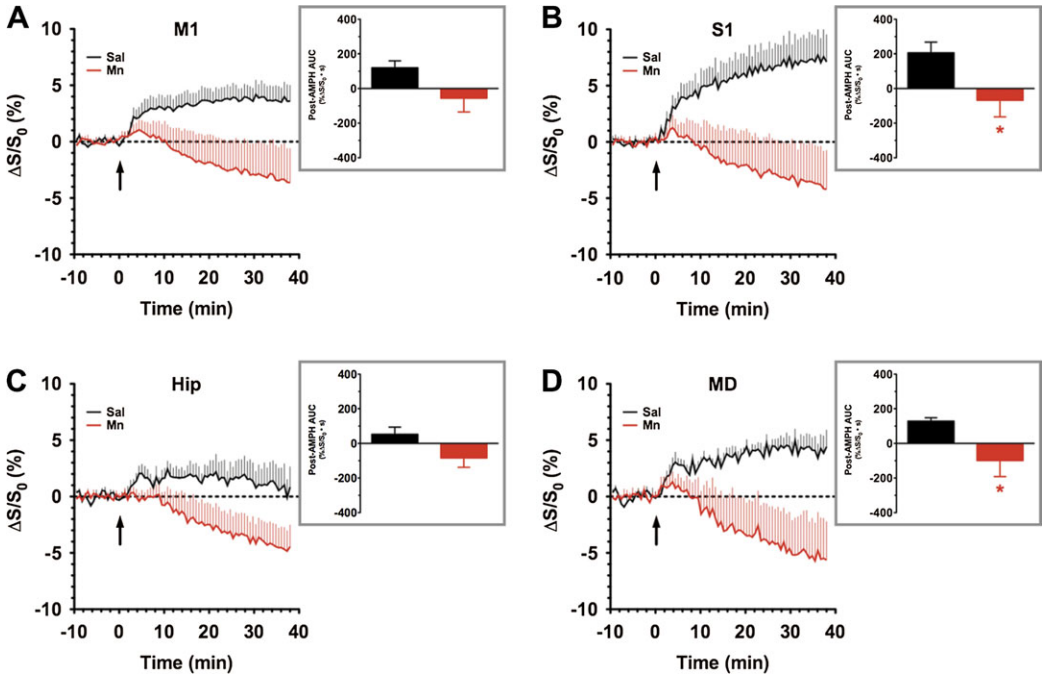

FIG. 6. ROI analyses of BOLD phMRI data obtained within the cortex and thalamus of saline- versus chronic Mn-treated subjects. Time series data represent mean $\%\Delta S/S_0$ in the ROI in response to AMPH injection (3 mg/kg, iv, arrow): (A) M1, (B) S1, (C)hippocampus, Hip, and (D) MD. Insets: Integration of post-AMPH time series data reveals a statistically significant decrease in the AMPH-induced BOLD response within the S1 and MD (AUC, $\%\Delta S/S_0 \bullet s$). Saline versus Mn: $*p < 0.05$, Student's *t*-test.

of suggestive trends from the time series data, the AUC for the AMPH-induced BOLD response in the hippocampus of Mn-treated subjects did not significantly differ from that of saline control (Fig. 6C, inset), despite the same trend toward a negative BOLD response. However, in the MD, a significant difference ($p < 0.05$) in AMPH-induced BOLD response was observed between Mn and saline pretreatment groups (Fig. 6D, inset), again as a result of a negative BOLD response to AMPH in the Mn-exposed group.

Mesocorticolimbic system. The mesocorticolimbic DA system plays a critical role in the etiology and progression of addictive disorders (Wise, 2005). DAergic neurons of the ventral tegmental area (VTA) project rostrally toward the mPFC and the nucleus accumbens (NAc). This system plays an important role in the pharmacological activity of psychostimulant drugs that act on DA in the CNS and because there is much overlap, synergy, and integration with the nigrostriatal system that is so significantly influenced by Mn, we examined the mesocorticolimbic system. Assessing the BOLD responses to AMPH stimulation within the NAc and mPFC, it became apparent that there was a high degree of heterogeneity in the response of each region. This was true regardless of the pretreatment condition. Thus, anterior and posterior ROIs in the NAc (NAc-A and NAc-P in Figs. 7A and 7B, respectively) and mPFC (mPFC-A and mPFC-P in Figs. 7C and 7D, respectively) were examined independently. In the anterior NAc, BOLD signals increased above baseline in response to AMPH injection in saline-treated, and to a slightly lesser extent, in Mn-treated subjects (Fig. 7A). The AMPH-induced BOLD response in the posterior NAc of both Mn- and saline-treated controls suffered from a high degree of temporal variation, likely stemming from the lack of stability in the baseline period for these voxels (Fig. 7B).

The response of the anterior mPFC to AMPH injection within saline-pretreated controls was surprising in that there was actually a modest decrease in the BOLD signal relative to predrug baseline; however, this decrease was even more pronounced in Mn-treated subjects (Fig. 7C). In contrast to the behavior of the anterior mPFC, the posterior mPFC exhibited a differential response to AMPH between Mn- versus saline-treated animals that was similar to the dissociated trends found in some of the basal ganglia and thalamocortical ROIs (Fig. 7D). Analysis of post-AMPH AUC values did not reveal any significant differences between Mn- versus saline-treated subjects in either the NAc or the mPFC, regardless of whether the regions were analyzed using average values from anterior and posterior slices or if the ROIs were analyzed separately (Figs. 7A–D, insets). BOLD signals in the VTA, like those from other ventral brain structures that were more distant from the RF surface coil, were found to exhibit a high degree of temporal variation (i.e., noise), regardless of pretreatment condition (Fig. 7E). Thus, experimental conditions precluded the possibility of measuring meaningful AMPH-induced BOLD signal changes within the pituitary gland, a structure known to accumulate Mn in rodents (Kuo *et al.*, 2005) and in primates

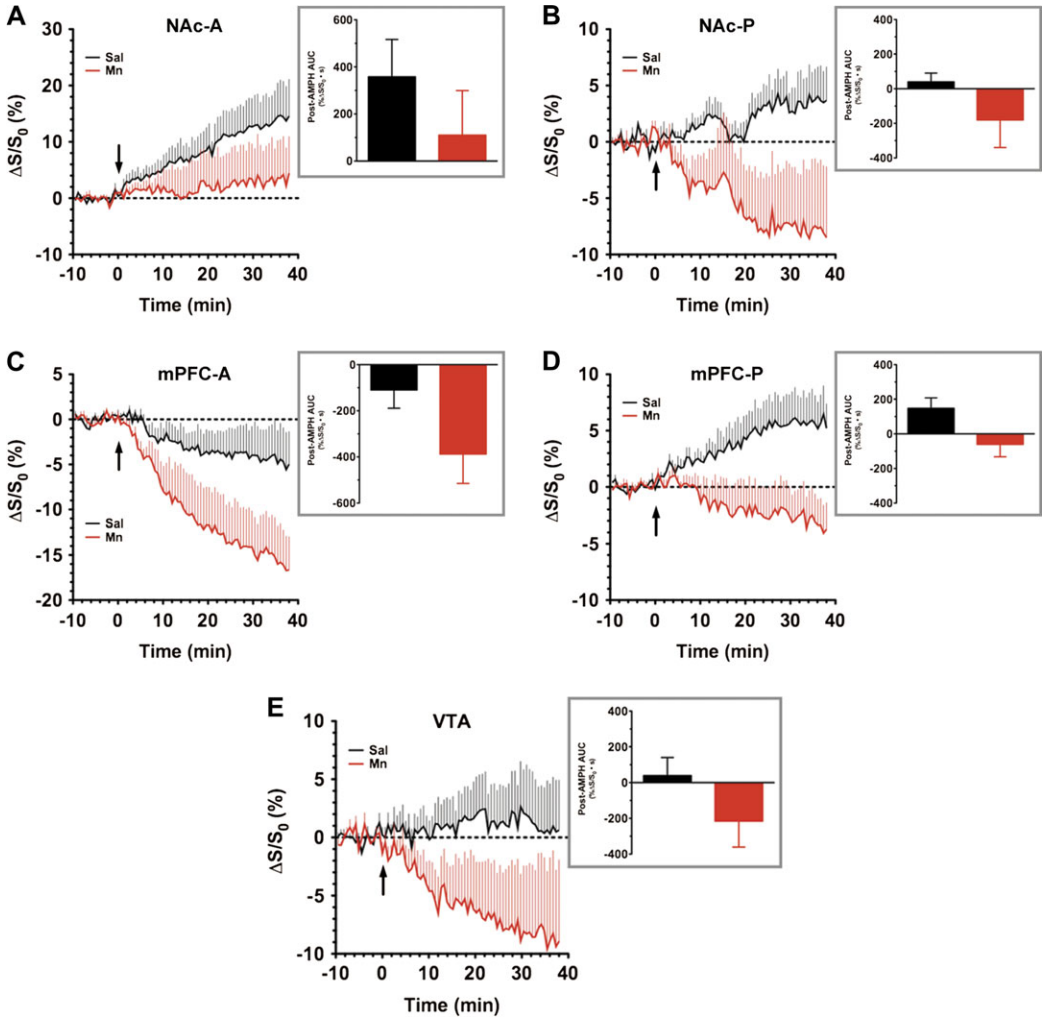

FIG. 7. ROI analyses of BOLD phMRI data obtained within the mesocorticolimbic DA system of saline- versus chronic Mn-treated subjects. Time series data represent mean $\%\Delta S/S_0$ in the ROI in response to AMPH injection (3 mg/kg, iv, arrow): (A) NAc-A, (B) NAc-P, (C) mPFC-A, (D) mPFC-P, and (E) VTA. Insets: Integration of post-AMPH time series data failed to show a statistically significant difference in the AMPH-induced BOLD response within each of the five regions, regardless of whether anterior and posterior ROIs were analyzed separately or in combination (AUC, $\%\Delta S/S_0 \bullet s$). Saline versus Mn: $p > 0.05$, Student's *t*-test.

(Newland *et al.*, 1989; Suzuki *et al.*, 2003), with a sufficient SNR.

DISCUSSION

The current study employed phMRI to assess the BOLD response to an acute systemic bolus injection of AMPH (3 mg/kg, ip) in an animal model of chronic Mn exposure as a means of investigating the overall functional status of the CNS after Mn intoxication. The treatment regimen employed in the current studies (5 mg Mn^{2+}/kg, iv, once weekly injection for 6 weeks) was intended to provide a low-to-moderate level of Mn deposition and accumulation (Fitsanakis *et al.*, 2008). This regimen resulted in an approximate doubling of Mn concentration within plasma ($p < 0.05$) and striatal tissue ($p > 0.05$) obtained from animals at the conclusion of MR scans. Notably, even with this relatively modest dosing regimen, animals in the Mn treatment group displayed a significant blunting, or even a switch from positive to negative, of the AMPH-evoked BOLD signal change in many brain areas compared to saline-treated control animals. Table 1 summarizes the results of ROI analyses for structures throughout the basal ganglia, cortex, and ventral midbrain. The regions of the brain most impacted by Mn were the GP, CPu, S1, MD, and SNc. Collectively, these data are (1) consistent with the known CNS toxicity profile associated with Mn exposure, (2) emphasize the role of DAergic neurons in Mn-induced neurotoxicity, and (3) establish the use of the phMRI response to AMPH as a novel tool to dynamically evaluate the underlying central pathophysiology resulting from Mn intoxication as well as potentially others toxicants known to target the basal ganglia.

TABLE 1
Summary of ROI Analysis of the AMPH-Induced BOLD phMRI Response within Select Brain Areas of Chronic Mn- versus Saline-Treated Animals

ROI	Saline AUC (mean ± SEM)	Mn AUC (mean ± SEM)	t ($df = 11$)	p
CPu	183.1 ± 45.5	−87.9 ± 94.6	2.441	0.0328*
GP	122.7 ± 39.9	−136.2 ± 85.9	2.557	0.0257*
Hippocampus	52.6 ± 41.4	−84.2 ± 54.1	1.954	0.0766
M1	120.1 ± 40.1	−56.0 ± 79.3	1.879	0.0869
MD	128.9 ± 19.2	−99.2 ± 92.6	2.231	0.0475*
mPFC	19.1 ± 62.9	−224.6 ± 97.9	2.011	0.0695
NAc	199 ± 86.7	−62.7 ± 141.7	1.509	0.1595
S1	206.5 ± 61.7	−68.15 ± 95.6	2.321	0.0405*
SNc	153.5 ± 90.7	−84.9 ± 62.7	2.217	0.0487*
STh	68.2 ± 55.2	−192.6 ± 105.9	2.073	0.0624
VTA	39.2 ± 101.0	−215.8 ± 145.1	1.394	0.1909

Note. Post-AMPH responses were integrated through time and the resulting AUC for each ROI subject. An unpaired two-tailed Student's t-test was then used to compare the AUCs (in units of mean ± SEM $\%\Delta S/S_0 \bullet s$) Mn- versus saline-treated groups.
*$p < 0.05$.

The main mechanism by which the BOLD mapping sequence used in the present study detects changes in neural activity is through changes in R2* associated with changes in blood susceptibility, which result from changes in deoxyhemoglobin concentration and blood volume. Furthermore, the BOLD phMRI method used to map brain activity in this study may also be sensitive to changes in longitudinal relaxation time (T1) and T2 under certain circumstances. We therefore conducted a prior study (Zhang *et al*., 2009) in which we confirmed that Mn treatment had little, if any, effect on T2 and that those effects were less than the variability in T2* between animals within and across groups at baseline, arising from macroscopic static magnetic field inhomogeneities. Furthermore, potential differences between groups in blood T1, T2, or Mn-associated differences in blood magnetic susceptibility were several orders of magnitude lower than can be detected by current BOLD fMRI methods. Thus, we are confident that the differences in response to AMPH observed in Mn-treated animals reflect biological differences rather than reflecting differences in the nature of the BOLD reporter response arising from additional contributions of higher Mn levels in the Mn-treated group.

Accumulating evidence in humans and in laboratory animals suggests that exposure to environmental toxicants, such as Mn, may contribute to the development and/or exacerbation of PD and other related neurodegenerative diseases (Di Monte, 2003). Recent investigation into the underlying neurobiology of manganism has uncovered mechanistic similarities between Mn-induced toxicity and PD. In both diseases, the neurobiological substrates involved seem to revolve around deficits in DA transmission. Areas of the CNS most sensitive to Mn deposition and neurotoxicity are metabolically active regions that are highly susceptible to oxidative stress. DAergic cells of the nigrostriatal pathway, which emanates from the SN and projects to the CPu (i.e., striatum), consume large amounts of adenosine triphosphate (ATP) to meet the metabolic demands on this circuit in mediating motor output from the basal ganglia (Klockgether and Turski, 1989). The SN, together with the GP and striatum, is targeted by Mn. At the subcellular level, within these regions, Mn disrupts mitochondrial ATP synthesis (Erikson *et al*., 2007; Fitsanakis *et al*., 2006). The mechanisms of neurodegeneration elicited by Mn and those associated with PD appear to be similar. Both diseases are characterized by mitochondrial dysfunction, oxidative stress, irregularities in signal transduction, aggregation of proteins, and the triggering of programmed cell death pathways (Aschner *et al*., 2007). Consistent with the above findings, the current data reveal that chronic low-level systemic exposure to Mn results in substantial buildup of this metal in the circulation and in brain tissue. This accumulation paralleled a noticeable blunting and even reversal of the sign of the AMPH-induced BOLD phMRI response, which was most pronounced in the basal ganglia and its corticothalamic inputs. Our findings of altered BOLD responsiveness in both the DAergic projection fields of the CPu and its downstream efferents (GP) are consistent with the high level of deposition of Mn in these structures. The altered response to AMPH in CPu is consistent with direct effects of Mn on DA neurotransmission. However, the effects seen in the GP may reflect one or both direct non-DAergic neurotoxicity in pallidal neurons and/or downstream consequences of impaired CPu outflow.

Psychostimulants such as AMPH enhance CNS DA transmission by stimulating transmitter release from synaptic vesicles and into the extracellular space (Sulzer *et al*., 2005). These effects are most pronounced within DAergic pathways such as the mesocorticolimbic and nigrostriatal systems that play critical roles in motivational salience, reinforcement, goal-directed behavior, and locomotor output (Koob, 2006; Wise, 2004). To conserve DA after its release, the DAT acts to reuptake excess transmitter into the cytosol where it can then be repackaged into synaptic vesicles (Amara and Sonders, 1998; Giros *et al*., 1996; Kahlig and Galli, 2003).

BOLD phMRI has been used to delineate responses to D and L stereoisomers of AMPH (Easton *et al*., 2007) as well as to differentiate responses to varying AMPH doses as well as agonist/antagonist pretreatment (Dixon *et al*., 2005). AMPH-evoked increases in extracellular DA, sampled with *in vivo* microdialysis of the striatum, are temporally and quantitatively well correlated with drug-induced increases in the BOLD signal measured in this region (Chen *et al*., 1997, 1999). Moreover, the AMPH-induced BOLD response measured by phMRI is also spatially linked to DAT binding with the PET radioligands [^{11}C]CFT (Chen *et al*., 1999). BOLD phMRI responses to AMPH have also been used to examine the central functional consequences of hypoinsulinemia within the striatum (Williams *et al*., 2007). These and many other studies

confirm the utility of the phMRI response to AMPH as a valuable *in vivo* probe of the overall functional status of central DAergic systems within small laboratory animals.

Previous studies in laboratory animals have investigated the links between repetitive exposure to Mn and neuroadaptations in monoamines, particularly DA. Studies in nonhuman primates (Bird *et al*., 1984; Eriksson *et al*., 1992b) and in rodents (Chandra and Shukla, 1981; Daniels and Abarca, 1991; Nam and Kim, 2008; Sloot and Gramsbergen, 1994; Sloot *et al*., 1994) suggest that chronic Mn intoxication produces considerable dysfunction of the DA system, especially in the basal ganglia. These effects are most often expressed as a reduced tissue concentration of DA, a reduction in the number and function of DA nerve terminals, a decrease in the number of receptors for DA, and/or a reduction in DAT binding. With regard to the latter, we were able to evaluate the functional status of DAT by use of AMPH, a compound that is known to act as a pseudosubstrate for DAT that is transported into DAergic neurons, where it depletes vesicular stores of DA to ultimately stimulate the release of DA into the synaptic cleft (Sulzer *et al*., 2005). Previous PET studies in nonhuman primates that had been repeatedly exposed to Mn had shown substantial decreases in DAT binding within the striatum (Eriksson *et al*., 1992b). Establishing the density of DAT in striatal tissue has been an important clinical end point for establishing the functional integrity of the nigrostriatal DA system (Pirker *et al*., 2002). PET and other nuclear imaging modalities such as single photon emission computed tomography with DAT-selective radioligands such as (1r)-2β-carboxymethoxy-3β-(4-iodophenyl) tropane (β-CIT) have been used to show that within PD patients who have a history of Mn exposure DAT levels are significantly reduced (Huang *et al*., 2003; Kim *et al*., 2002).

When administered at low doses over prolonged periods of time, Mn exerts some of its neurotoxic effects via actions that are mediated by the DAT (Guilarte *et al*., 2006, 2008). Located perisynaptically in the plasma membrane of DA-releasing neurons within the striatum (Cass *et al*., 1992; Ciliax *et al*., 1995; Nirenberg *et al*., 1996), DAT functions as the primary mechanism for reuptake of DA released into the extracellular *milieu* during synaptic transmission (Amara and Sonders, 1998; Giros *et al*., 1996; Kahlig and Galli, 2003; Williams and Galli, 2006). The sites at which Mn may act to alter the AMPH-induced BOLD response are numerous and evidence in support of its action at any or multiple sites at present is largely speculative. The effect of Mn may occur at (1) the level of basal blood flow, metabolism, and/or the level of vascular coupling, for which presently no data exist; (2) alternatively, Mn may depress AMPH-evoked DA release by changing the distribution of DAT, reducing its extracellular localization in favor of increased intracellular concentration, or possibly a net reduction in DAT in both compartments; (3) Mn may alter the presynaptic function of DAT as recently posited by Guilarte *et al*. (2006, 2008). In this scenario, Mn would be expected to decrease cytosolic and/or vesicular DA levels, reducing its net release; (4) it has also yet to be determined whether Mn can alter the function of proteins essential for vesicular neurotransmitter release, such as SNARE, and the docking of vesicular monoamines to the cytosolic membrane; (5) Mn may also compete with the uptake of DA at the DAT, thus reducing intracellular DA levels, resulting in depressed methamphetamine-evoked response. Notably, DAT inhibitors, such as cocaine or GBR12909, reduce uptake of Mn in striatal tissue (Anderson *et al*., 2007; Ingersoll *et al*., 1999), and Mn effectively inhibits DA uptake in striatal synaptosomes (Anderson *et al*., 2007; Chen *et al*., 2006); (6) the altered DAergic response to AMPH-evoked challenge may also reflect DAergic cell stress and/or death, a known consequence of Mn exposure. Mn is known to selectively affect pathways intrinsic to the basal ganglia, decreasing DA levels in the basal ganglia of intoxicated monkeys and rats (Bird *et al*., 1984; Brouillet *et al*., 1993; Eriksson *et al*., 1992a; Guilarte *et al*., 2008). Finally, (7) Mn may modify the dynamic range at which AMPH elicits an increase in extracellular DA, thus effectively reducing its release. However, data in support of this theory do not presently exist.

In summary, the current work used the BOLD phMRI response to AMPH—a psychostimulant that evokes the release of DA from the nerve terminals, thus acting as an indirect agonist at DA receptors (Sulzer *et al*., 2005)—to assess the functional status of neural pathways and brain areas that are known to undergo degeneration as a result of PD and/or Mn neurotoxicity. The studies reported herein establish that Mn-treated animals exhibit widespread modulation of the AMPH-induced BOLD response throughout several CNS areas, including those known to preferentially accumulate and show exquisite sensitivity to elevated Mn levels. The findings provide novel information not only on the neural deficits associated with Mn neuropathology but also establish phMRI as a tool for the assessment of DAergic vulnerability using AMPH-evoked BOLD responses as a readout for the functional status of DAergic systems. Furthermore, the present study reconciles earlier reports on nigrostriatal degeneration and the observations of impaired striatal impairment (Guilarte *et al*., 2006, 2008; Olanow, 2004), suggesting that striatally accumulated Mn broadly impacts basal ganglia function subserving multiple circuitry systems affected both in PD and in parkinsonism-like conditions. Future studies utilizing BOLD technology may be profitably applied to assessment of the temporal relationship between Mn exposure and DAergic dysfunction shedding further light on regional specificity associated with exposure to this metal.

FUNDING

National Institutes of Health grants (NS057223 to D.M., EB001628 and CA068485 to J.C.G., and ES010563 to M.A.).

ACKNOWLEDGMENTS

The authors thank Chad Quarles, Baxter Rogers, Saikat Sengupta, Richard Baheza, Heather Scott, Jarrod True, and Ken Wilkens of the Vanderbilt University Institute of Imaging Science for their exceptional analytical expertise and technical assistance.

REFERENCES

Al-Bader, A. A., Mosawi, M. H., Hussain, T. A., and Dashti, H. M. (1997). Effect of dietary selenium, zinc and allopurinol supplements on plasma and tissue manganese levels in rats with thioacetamide [correction of thiocetamide]-induced liver cirrhosis. *Mol. Cell. Biochem.* **173,** 121–125.

Amara, S. G., and Sonders, M. S. (1998). Neurotransmitter transporters as molecular targets for addictive drugs. *Drug Alcohol Depend.* **51,** 87–96.

Anderson, J. G., Cooney, P. T., and Erikson, K. M. (2007). Inhibition of DAT function attenuates manganese accumulation in the globus pallidus. *Environ. Toxicol. Pharmacol.* **23,** 179–184.

Arthurs, O. J., and Boniface, S. (2002). How well do we understand the neural origins of the fMRI BOLD signal? *Trends Neurosci.* **25,** 27–31.

Aschner, M., and Aschner, J. L. (1991). Manganese neurotoxicity: cellular effects and blood-brain barrier transport. *Neurosci. Biobehav. Rev.* **15,** 333–340.

Aschner, M., Guilarte, T. R., Schneider, J. S., and Zheng, W. (2007). Manganese: recent advances in understanding its transport and neurotoxicity. *Toxicol. Appl. Pharmacol.* **221,** 131–147.

Bird, E. D., Anton, A. H., and Bullock, B. (1984). The effect of manganese inhalation on basal ganglia dopamine concentrations in rhesus monkey. *Neurotoxicology* **5,** 59–65.

Brooks, D. J., Ibanez, V., Sawle, G. V., Quinn, N., Lees, A. J., Mathias, C. J., Bannister, R., Marsden, C. D., and Frackowiak, R. S. (1990). Differing patterns of striatal 18F-dopa uptake in Parkinson's disease, multiple system atrophy, and progressive supranuclear palsy. *Ann. Neurol.* **28,** 547–555.

Brouillet, E. P., Shinobu, L., McGarvey, U., Hochberg, F., and Beal, M. F. (1993). Manganese injection into the rat striatum produces excitotoxic lesions by impairing energy metabolism. *Exp. Neurol.* **120,** 89–94.

Burton, N. C., and Guilarte, T. R. (2009). Manganese neurotoxicity: lessons learned from longitudinal studies in nonhuman primates. *Environ. Health Perspect.* **117,** 325–332.

Buxton, R. B., Uludag, K., Dubowitz, D. J., and Liu, T. T. (2004). Modeling the hemodynamic response to brain activation. *Neuroimage* **23**(Suppl. 1), S220–S233.

Calne, D. B., Chu, N. S., Huang, C. C., Lu, C. S., and Olanow, W. (1994). Manganism and idiopathic parkinsonism: similarities and differences. *Neurology* **44,** 1583–1586.

Cass, W. A., Gerhardt, G. A., Mayfield, R. D., Curella, P., and Zahniser, N. R. (1992). Differences in dopamine clearance and diffusion in rat striatum and nucleus accumbens following systemic cocaine administration. *J. Neurochem.* **59,** 259–266.

Chandra, S. V., and Shukla, G. S. (1981). Concentrations of striatal catecholamines in rats given manganese chloride through drinking water. *J. Neurochem.* **36,** 683–687.

Chen, M. K., Lee, J. S., McGlothan, J. L., Furukawa, E., Adams, R. J., Alexander, M., Wong, D. F., and Guilarte, T. R. (2006). Acute manganese administration alters dopamine transporter levels in the non-human primate striatum. *Neurotoxicology* **27,** 229–236.

Chen, Y. C., Galpern, W. R., Brownell, A. L., Matthews, R. T., Bogdanov, M., Isacson, O., Keltner, J. R., Beal, M. F., Rosen, B. R., and Jenkins, B. G. (1997). Detection of dopaminergic neurotransmitter activity using pharmacologic MRI: correlation with PET, microdialysis, and behavioral data. *Magn. Reson. Med.* **38,** 389–398.

Chen, Y. I., Brownell, A. L., Galpern, W., Isacson, O., Bogdanov, M., Beal, M. F., Livni, E., Rosen, B. R., and Jenkins, B. G. (1999). Detection of dopaminergic cell loss and neural transplantation using pharmacological MRI, PET and behavioral assessment. *Neuroreport* **10,** 2881–2886.

Ciliax, B. J., Heilman, C., Demchyshyn, L. L., Pristupa, Z. B., Ince, E., Hersch, S. M., Niznik, H. B., and Levey, A. I. (1995). The dopamine transporter: immunochemical characterization and localization in brain. *J. Neurosci.* **15,** 1714–1723.

Cotterill, R. M. (2001). Cooperation of the basal ganglia, cerebellum, sensory cerebrum and hippocampus: possible implications for cognition, consciousness, intelligence and creativity. *Prog. Neurobiol.* **64,** 1–33.

Cox, R. W. (1996). AFNI: software for analysis and visualization of functional magnetic resonance neuroimages. *Comput. Biomed. Res.* **29,** 162–173.

Daniels, A. J., and Abarca, J. (1991). Effect of intranigral Mn2+ on striatal and nigral synthesis and levels of dopamine and cofactor. *Neurotoxicol. Teratol.* **13,** 483–487.

Di Monte, D. A. (2003). The environment and Parkinson's disease: is the nigrostriatal system preferentially targeted by neurotoxins? *Lancet Neurol.* **2,** 531–538.

Dixon, A. L., Prior, M., Morris, P. M., Shah, Y. B., Joseph, M. H., and Young, A. M. (2005). Dopamine antagonist modulation of amphetamine response as detected using pharmacological MRI. *Neuropharmacology* **48,** 236–245.

Easton, N., Marshall, F., Fone, K. C., and Marsden, C. A. (2007). Differential effects of the D- and L- isomers of amphetamine on pharmacological MRI BOLD contrast in the rat. *Psychopharmacology (Berl.)* **193,** 11–30.

Erikson, K. M., Dorman, D. C., Lash, L. H., and Aschner, M. (2007). Manganese inhalation by rhesus monkeys is associated with brain regional changes in biomarkers of neurotoxicity. *Toxicol. Sci.* **97,** 459–466.

Eriksson, H., Gillberg, P. G., Aquilonius, S. M., Hedstrom, K. G., and Heilbronn, E. (1992a). Receptor alterations in manganese intoxicated monkeys. *Arch. Toxicol.* **66,** 359–364.

Eriksson, H., Tedroff, J., Thuomas, K. A., Aquilonius, S. M., Hartvig, P., Fasth, K. J., Bjurling, P., Langstrom, B., Hedstrom, K. G., and Heilbronn, E. (1992b). Manganese induced brain lesions in Macaca fascicularis as revealed by positron emission tomography and magnetic resonance imaging. *Arch. Toxicol.* **66,** 403–407.

Ferraz, H. B., Bertolucci, P. H., Pereira, J. S., Lima, J. G., and Andrade, L. A. (1988). Chronic exposure to the fungicide maneb may produce symptoms and signs of CNS manganese intoxication. *Neurology* **38,** 550–553.

Fitsanakis, V. A., Au, C., Erikson, K. M., and Aschner, M. (2006). The effects of manganese on glutamate, dopamine and gamma-aminobutyric acid regulation. *Neurochem. Int.* **48,** 426–433.

Fitsanakis, V. A., Zhang, N., Anderson, J. G., Erikson, K. M., Avison, M. J., Gore, J. C., and Aschner, M. (2008). Measuring brain manganese and iron accumulation in rats following 14 weeks of low-dose manganese treatment using atomic absorption spectroscopy and magnetic resonance imaging. *Toxicol. Sci.* **103,** 116–124.

Giros, B., Jaber, M., Jones, S. R., Wightman, R. M., and Caron, M. G. (1996). Hyperlocomotion and indifference to cocaine and amphetamine in mice lacking the dopamine transporter. *Nature* **379,** 606–612.

Gore, J. C. (2003). Principles and practice of functional MRI of the human brain. *J. Clin. Invest.* **112,** 4–9.

Guilarte, T. R., Burton, N. C., McGlothan, J. L., Verina, T., Zhou, Y., Alexander, M., Pham, L., Griswold, M., Wong, D. F., Syversen, T., *et al.* (2008). Impairment of nigrostriatal dopamine neurotransmission by manganese is mediated by pre-synaptic mechanism(s): implications to manganese-induced parkinsonism. *J. Neurochem.* **107,** 1236–1247.

Guilarte, T. R., Chen, M. K., McGlothan, J. L., Verina, T., Wong, D. F., Zhou, Y., Alexander, M., Rohde, C. A., Syversen, T., Decamp, E., *et al*. (2006). Nigrostriatal dopamine system dysfunction and subtle motor deficits in manganese-exposed non-human primates. *Exp. Neurol.* **202,** 381–390.

Huang, C. C., Chu, N. S., Lu, C. S., Chen, R. S., and Calne, D. B. (1998). Long-term progression in chronic manganism: ten years of follow-up. *Neurology* **50,** 698–700.

Huang, C. C., Weng, Y. H., Lu, C. S., Chu, N. S., and Yen, T. C. (2003). Dopamine transporter binding in chronic manganese intoxication. *J. Neurol.* **250,** 1335–1339.

Ingersoll, R. T., Montgomery, E. B. J., and Aposhian, H. V. (1999). Central nervous system toxicity of manganese. II: cocaine or reserpine inhibit manganese concentration in the rat brain. *Neurotoxicology* **20,** 467–476.

Kahlig, K. M., and Galli, A. (2003). Regulation of dopamine transporter function and plasma membrane expression by dopamine, amphetamine, and cocaine. *Eur. J. Pharmacol.* **479,** 153–158.

Kim, Y. (2006). Neuroimaging in manganism. *Neurotoxicology* **27,** 369–372.

Kim, Y., Kim, J. M., Kim, J. W., Yoo, C. I., Lee, C. R., Lee, J. H., Kim, H. K., Yang, S. O., Chung, H. K., Lee, D. S., *et al*. (2002). Dopamine transporter density is decreased in parkinsonian patients with a history of manganese exposure: what does it mean? *Mov. Disord.* **17,** 568–575.

Klockgether, T., and Turski, L. (1989). Excitatory amino acids and the basal ganglia: implications for the therapy of Parkinson's disease. *Trends Neurosci.* **12,** 285–286.

Koob, G. F. (2006). The neurobiology of addiction: a neuroadaptational view relevant for diagnosis. *Addiction* **101**(Suppl. 1), 23–30.

Kuo, Y. T., Herlihy, A. H., So, P. W., Bhakoo, K. K., and Bell, J. D. (2005). *In vivo* measurements of T1 relaxation times in mouse brain associated with different modes of systemic administration of manganese chloride. *J. Magn. Reson. Imaging* **21,** 334–339.

Leenders, K. L., Salmon, E. P., Tyrrell, P., Perani, D., Brooks, D. J., Sager, H., Jones, T., Marsden, C. D., and Frackowiak, R. S. (1990). The nigrostriatal dopaminergic system assessed in vivo by positron emission tomography in healthy volunteer subjects and patients with Parkinson's disease. *Arch. Neurol.* **47,** 1290–1298.

Logothetis, N. K. (2003). The underpinnings of the BOLD functional magnetic resonance imaging signal. *J Neurosci* **23,** 3963–3971.

Logothetis, N. K., and Pfeuffer, J. (2004). On the nature of the BOLD fMRI contrast mechanism. *Magn. Reson. Imaging* **22,** 1517–1531.

Mahoney, J. P., and Small, W. J. (1968). Studies on manganese. 3. The biological half-life of radiomanganese in man and factors which affect this half-life. *J. Clin. Invest.* **47,** 643–653.

McDonald, M. C., d'Emmanuele di Villa Bianca, R., Wayman, N. S., Pinto, A., Sharpe, M. A., Cuzzocrea, S., Chatterjee, P. K., and Thiemermann, C. (2003). A superoxide dismutase mimetic with catalase activity (EUK-8) reduces the organ injury in endotoxic shock. *Eur. J. Pharmacol.* **466,** 181–189.

Mergler, D. (1999). Neurotoxic effects of low level exposure to manganese in human populations. *Environ. Res.* **80,** 99–102.

Muller-Gartner, H. W. (1998). Imaging techniques in the analysis of brain function and behaviour. *Trends Biotechnol.* **16,** 122–130.

Nam, J., and Kim, K. (2008). Abnormal motor function and the expression of striatal dopamine D2 receptors in manganese-treated mice. *Biol. Pharm. Bull.* **31,** 1894–1897.

Narita, K., Kawasaki, F., and Kita, H. (1990). Mn and Mg influxes through Ca channels of motor nerve terminals are prevented by verapamil in frogs. *Brain Res.* **510,** 289–295.

Newland, M. C., Ceckler, T. L., Kordower, J. H., and Weiss, B. (1989). Visualizing manganese in the primate basal ganglia with magnetic resonance imaging. *Exp. Neurol.* **106,** 251–258.

Nirenberg, M. J., Vaughan, R. A., Uhl, G. R., Kuhar, M. J., and Pickel, V. M. (1996). The dopamine transporter is localized to dendritic and axonal plasma membranes of nigrostriatal dopaminergic neurons. *J. Neurosci.* **16,** 436–447.

Ogawa, S., Lee, T. M., Kay, A. R., and Tank, D. W. (1990). Brain magnetic resonance imaging with contrast dependent on blood oxygenation. *Proc. Natl. Acad. Sci. U.S.A* **87,** 9868–9872.

Olanow, C. W. (2004). Manganese-induced parkinsonism and Parkinson's disease. *Ann. N. Y. Acad. Sci.* **1012,** 209–223.

Pal, P. K., Samii, A., and Calne, D. B. (1999). Manganese neurotoxicity: a review of clinical features, imaging and pathology. *Neurotoxicology* **20,** 227–238.

Park, N. H., Park, J. K., Choi, Y., Yoo, C. I., Lee, C. R., Lee, H., Kim, H. K., Kim, S. R., Jeong, T. H., Park, J., *et al*. (2003). Whole blood manganese correlates with high signal intensities on T1-weighted MRI in patients with liver cirrhosis. *Neurotoxicology* **24,** 909–915.

Paxinos, G., and Watson, C. (1998). The Rat Brain in Stereotaxic Coordinates, (4th ed). Academic Press, New York.

Perl, D. P., and Olanow, C. W. (2007). The neuropathology of manganese-induced parkinsonism. *J. Neuropathol. Exp. Neurol.* **66,** 675–682.

Pirker, W., Djamshidian, S., Asenbaum, S., Gerschlager, W., Tribl, G., Hoffmann, M., and Brucke, T. (2002). Progression of dopaminergic degeneration in Parkinson's disease and atypical parkinsonism: a longitudinal beta-CIT SPECT study. *Mov. Disord.* **17,** 45–53.

Racette, B. A., Antenor, J. A., McGee-Minnich, L., Moerlein, S. M., Videen, T. O., Kotagal, V., and Perlmutter, J. S. (2005). [18F]FDOPA PET and clinical features in parkinsonism due to manganism. *Mov. Disord.* **20,** 492–496.

Racette, B. A., McGee-Minnich, L., Moerlein, S. M., Mink, J. W., Videen, T. O., and Perlmutter, J. S. (2001). Welding-related parkinsonism: clinical features, treatment, and pathophysiology. *Neurology* **56,** 8–13.

Shinotoh, H., Snow, B. J., Chu, N. S., Huang, C. C., Lu, C. S., Lee, C., Takahashi, H., and Calne, D. B. (1997). Presynaptic and postsynaptic striatal dopaminergic function in patients with manganese intoxication: a positron emission tomography study. *Neurology* **48,** 1053–1056.

Shinotoh, H., Snow, B. J., Hewitt, K. A., Pate, B. D., Doudet, D., Nugent, R., Perl, D. P., Olanow, W., and Calne, D. B. (1995). MRI and PET studies of manganese-intoxicated monkeys. *Neurology* **45,** 1199–1204.

Sloot, W. N., and Gramsbergen, J. B. (1994). Axonal transport of manganese and its relevance to selective neurotoxicity in the rat basal ganglia. *Brain Res.* **657,** 124–132.

Sloot, W. N., van der Sluijs-Gelling, A. J., and Gramsbergen, J. B. (1994). Selective lesions by manganese and extensive damage by iron after injection into rat striatum or hippocampus. *J. Neurochem.* **62,** 205–216.

Stepens, A., Logina, I., Liguts, V., Aldins, P., Eksteina, I., Platkajis, A., Martinsone, I., Terauds, E., Rozentale, B., and Donaghy, M. (2008). A parkinsonian syndrome in methcathinone users and the role of manganese. *N. Engl. J. Med.* **358,** 1009–1017.

Steward, C. A., Marsden, C. A., Prior, M. J., Morris, P. G., and Shah, Y. B. (2005). Methodological considerations in rat brain BOLD contrast pharmacological MRI. *Psychopharmacology (Berl.)* **180,** 687–704.

Sulzer, D., Sonders, M. S., Poulsen, N. W., and Galli, A. (2005). Mechanisms of neurotransmitter release by amphetamines: a review. *Prog. Neurobiol.* **75,** 406–433.

Suzuki, H., Takanashi, J., Saeki, N., and Kohno, Y. (2003). Temporal parenteral nutrition in children causing T1 shortening in the anterior pituitary gland and globus pallidus. *Neuropediatrics* **34,** 200–204.

Takeda, A. (2003). Manganese action in brain function. *Brain Res. Brain Res. Rev.* **41,** 79–87.

Takeda, A., Sotogaku, N., and Oku, N. (2002). Manganese influences the levels of neurotransmitters in synapses in rat brain. *Neuroscience* **114,** 669–674.

Wichmann, T., and DeLong, M. R. (2003). Functional neuroanatomy of the basal ganglia in Parkinson's disease. *Adv. Neurol.* **91,** 9–18.

Williams, J. M., and Galli, A. (2006). The dopamine transporter: a vigilant border control for psychostimulant action. *Handb. Exp. Pharmacol.* **175,** 215–232.

Williams, J. M., Owens, W. A., Turner, G. H., Saunders, C., Dipace, C., Blakely, R. D., France, C. P., Gore, J. C., Daws, L. C., Avison, M. J., *et al.* (2007). Hypoinsulinemia regulates amphetamine-induced reverse transport of dopamine. *PLoS Biol.* **5,** 2369–2378.

Wise, R. A. (2004). Dopamine, learning and motivation. *Nat. Rev. Neurosci.* **5,** 483–494.

Wise, R. A. (2005). Forebrain substrates of reward and motivation. *J. Comp. Neurol.* **493,** 115–121.

Wise, R. G., and Tracey, I. (2006). The role of fMRI in drug discovery. *J. Magn. Reson. Imaging* **23,** 862–876.

Wolters, E. C., Huang, C. C., Clark, C., Peppard, R. F., Okada, J., Chu, N. S., Adam, M. J., Ruth, T. J., Li, D., and Calne, D. B. (1989). Positron emission tomography in manganese intoxication. *Ann. Neurol.* **26,** 647–651.

Xu, X. R., Li, H. B., Wang, W. H., and Gu, J. D. (2005). Decolorization of dyes and textile wastewater by potassium permanganate. *Chemosphere* **59,** 893–898.

Zhang, N., Fitsanakis, V. A., Erikson, K. M., Aschner, M., Avison, M. J., and Gore, J. C. (2009). A model for the analysis of competitive relaxation effects of manganese and iron in vivo. *NMR Biomed.* **22,** 391–404.